Structure, Vol. 13, 43–54, January, 2005, ©2005 Elsevier Ltd All rights reserved. DOI 10.1016/j.str.2004.10.012

X-Ray Structure of a Rex-Family Repressor/NADH Complex Insights into the Mechanism of Redox Sensing

E. Allen Sickmier,[1] Dimitris Brekasis,[2] Shanthi Paranawithana,[1] Jeffrey B. Bonanno,[3,4] Mark S.B. Paget,[2] Stephen K. Burley,[3,4,*] and Clara L. Kielkopf[1,3,*]

[1]Department of Biochemistry and Molecular Biology
Johns Hopkins Bloomberg School of Public Health
Baltimore, Maryland 21205

[2]Department of Biochemistry
University of Sussex
Falmer, Brighton BN1 9QG
United Kingdom

[3]The Rockefeller University and Howard Hughes Medical Institute
1230 York Avenue
New York, New York 10021

Summary

The redox-sensing repressor Rex regulates transcription of respiratory genes in response to the intracellular NADH/NAD$^+$ redox poise. As a step toward elucidating the molecular mechanism of NADH/NAD$^+$ sensing, the X-ray structure of *Thermus aquaticus* Rex (T-Rex) bound to effector NADH has been determined at 2.9 Å resolution. The fold of the C-terminal domain of T-Rex is characteristic of NAD(H)-dependent enzymes, whereas the N-terminal domain is similar to a winged helix DNA binding motif. T-Rex dimerization is primarily mediated by "domain-swapped" α helices. Each NADH molecule binds to the C-terminal domain near the dimer interface. In contrast to NAD(H)-dependent enzymes, the nicotinamide is deeply buried within a hydrophobic pocket that appears to preclude substrate entry. We show that T-Rex binds to the Rex operator, and NADH but not NAD$^+$ inhibits T-Rex/DNA binding activity. A mechanism for redox sensing by Rex family members is proposed by analogy with domain closure of NAD(H)-dependent enzymes.

Introduction

Aerobic organisms depend on a continuous supply of molecular oxygen primarily to act as a terminal electron acceptor during respiration. However, environmental oxygen levels can vary widely, and so cells have evolved elaborate mechanisms for sensing and adapting to these changes. Bacteria use a wide variety of sensors to continually monitor oxygen levels and cellular redox state and then transduce these signals into biological responses through induced conformational changes in regulatory proteins or enzymes. Adaptive responses to oxygen limitation include the repression of enzymes of the citric acid cycle, the production of alternative terminal oxidases with higher affinity for oxygen, and, in facultative bacteria, the production of enzymes that take advantage of different electron acceptors such as nitrate or fumarate (Patschkowski et al., 2000). Oxygen can also serve to regulate or impact several other processes including taxis (Taylor et al., 1999), pathogenesis (Brook, 2002; Murdoch, 1998; Park et al., 2003), industrial fermentation (Flores et al., 1997; Sassi et al., 1996), bioremediation (Van Hamme et al., 2003), and nitrogen fixation (Dixon and Kahn, 2004). Much progress has been made in identifying and characterizing the regulatory systems involved in sensing and responding to oxygen changes. Regulators can be broadly divided into those that sense oxygen directly, including the iron-sulfur cluster-containing sensor FNR (Jordan et al., 1997; Khoroshilova et al., 1997) and the haem-based sensor HemAT (Zhang and Phillips, 2003), and those that monitor the level or redox state of particular cellular metabolites. An example of the latter is the ArcB-ArcA two component system. The sensor kinase ArcB is thought to sense the redox state of the membrane-bound quinone pool, which shifts from an oxidized to a reduced state during oxygen limitation. Since oxidized but not reduced quinones inhibit the autophosphorylation of ArcB, oxygen limitation stimulates the ArcB-dependent phosphorylation of the response regulator ArcA (Georgellis et al., 2001).

Given its different metabolic fates under anaerobic versus aerobic conditions, NADH is particularly well suited to regulate transcriptional activity in response to changes in cellular redox balance. During catabolism of fuel molecules, NAD$^+$ is reduced to NADH. Under aerobic conditions, NADH is reoxidized to NAD$^+$ by the electron transport chain with concurrent reduction of molecular oxygen to water. In contrast, when the oxygen supply is limited, NAD$^+$ is regenerated through reduction of metabolic intermediates or alternative electron acceptors. Under steady-state conditions, the cytoplasmic concentration of free NAD$^+$ is much greater than that of its NADH counterpart (Williamson et al., 1967); hence, the relative fluctuations in free NADH levels are more dependent on the cellular redox state than on reciprocal changes in the NAD$^+$ concentration.

Recently, a novel redox-sensing repressor was discovered in *Streptomyces coelicolor* (Rex) that represses transcription of respiratory chain components in response to changes in the intracellular NADH/NAD$^+$ ratio (Brekasis and Paget, 2003). Rex is one member of a conserved family that is widespread among gram-positive bacteria, including the human pathogens *Bacillus anthracis* (anthrax), *Streptococcus pneumoniae* (pneumonia), and *Clostridium tetani* (lockjaw) (Figure 1A). Although both reduced and oxidized forms of NAD(H) dinucleotide bind to Rex, NADH but not NAD$^+$ inhibits DNA binding. The DNA target site of Rex (*R*ex *op*erator, ROP) is an inverted repeat found upstream of several genes encoding respiratory proteins, including cytochrome *bd* terminal oxidase, heme biosynthetic enzymes, NADH dehydrogenase, and Rex itself. Thus, when oxygen is limiting, the lowered respiratory rate is

*Correspondence: sburley@stromix.com (S.K.B.); ckielkop@jhsph.edu (C.L.K.)

[4]Present address: Structural GenomiX Inc., 10505 Roselle Street, San Diego, California 92121.

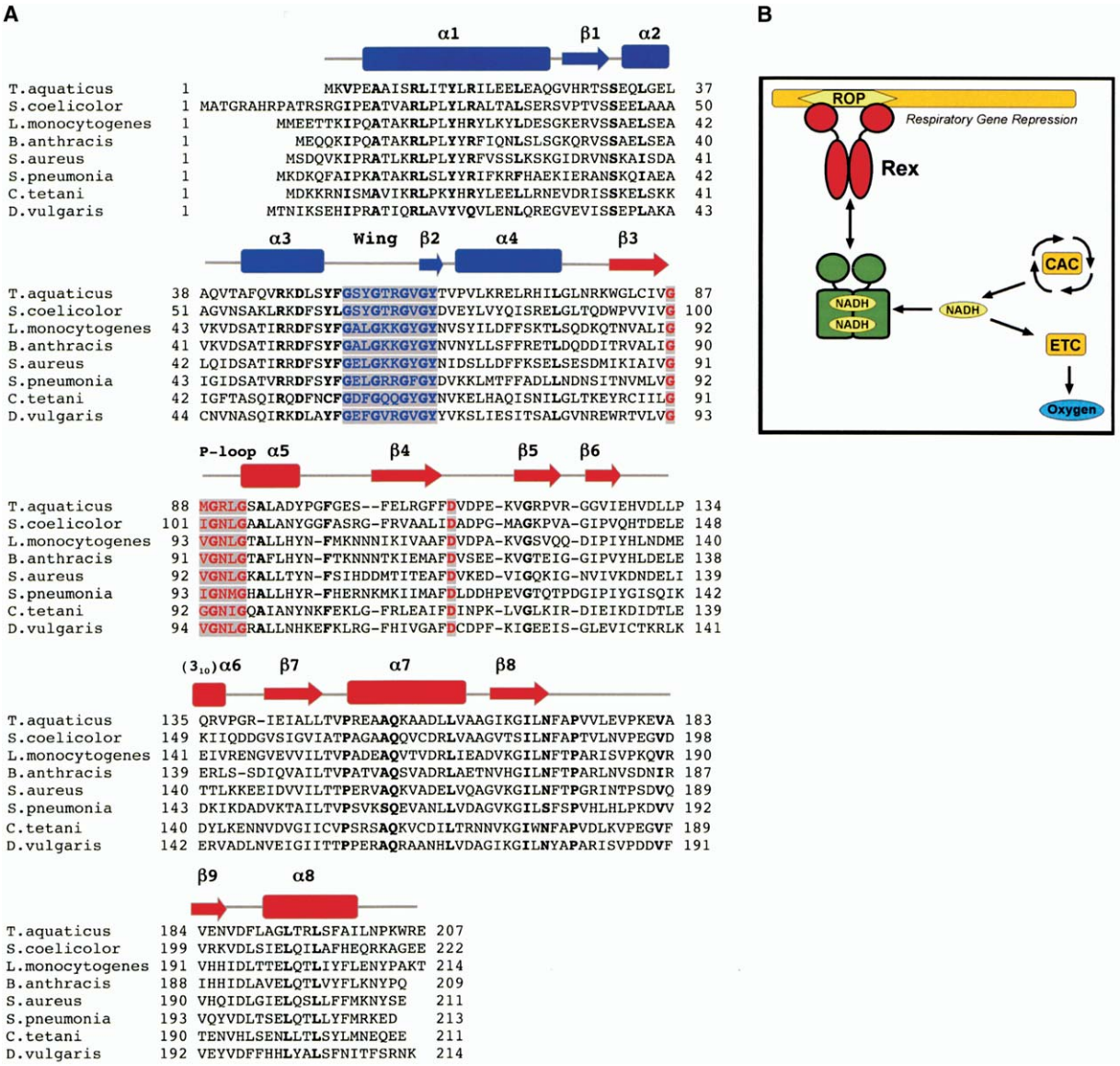

Figure 1. Function of the Rex Family

(A) Sequence alignment of representative members of the Rex family of transcription factors. *Thermus aquaticus* (Q9X2V5, T-Rex), *Streptomyces coelicolor* (Q9WX14, S-Rex), *Listeria monocytogenes* (CAD00150), *Bacillus anthracis* (Q81VE5), *Staphyloccocus aureus* (P60385), *Streptoccocus pneumoniae* (Q97QV8), *Clostridium tetani* (Q891F1), *Desulfovibrio vulgaris* (YP_010137). A unique C-terminal S-Rex extension (S-Rex residues 223–258) has been omitted for the sake of clarity. Residues that are identical in at least seven of the eight sequences are shown in bold. The Gly-rich signature motif of the Rossmann fold (red), the conserved Asp residue that distinguishes NADH from NADPH (red), and the conserved wing segment (blue) are shaded. T-Rex secondary structural elements observed in our X-ray structure are indicated above the sequences in blue or red for the WH or NAD(H) binding domains, respectively.

(B) Schematic overview of Rex control of respiratory gene transcription in response to the NADH/NAD$^+$ ratio. The target DNA is colored gold, the DNA-bound state of Rex is shown in red, the NADH-bound form in green. NAD, nicotinamide adenine dinucleotide; ROP, Rex operator; CAC, citric acid cycle; ETC, electron transport chain.

thought to cause NADH levels to rise, allowing NADH to replace NAD$^+$ bound to Rex, presumably triggering a conformational change that inhibits DNA binding. The reduced DNA binding affinity of the Rex/NADH complex removes the repressor from ROP sites so that genes are induced to ensure more efficient oxygen use (cytochrome *bd* terminal oxidase) and to recycle the excess NADH (NADH dehydrogenase; Figure 1B).

In eukaryotes, the structural basis of NAD(H)-dependent transcriptional regulation is understood for several pathways, including the transcriptional corepressor CtBP and the sirtuin (SIR2) protein deacetylases. The structures of CtBP/NAD(H) and CtBP/NADH/peptide complexes (Kumar et al., 2002; Nardini et al., 2003) reveal that binding of the dinucleotide to CtBP promotes formation of a closed dimeric conformation in which CtBP influences cell differentiation and development by selectively recognizing multimeric protein partners. Several structures of SIR2 family members provide insights into the mechanism of gene silencing by NAD$^+$-dependent histone deacetylation (Avalos et al., 2004, 2002; Chang et al., 2002; Finnin et al., 2001; Min et al., 2001;

Zhao et al., 2003a, 2003b) via a reaction that consumes NAD^+ and releases nicotinamide and *O*-acetyl ADP ribose as products (Blander and Guarente, 2004). Currently, our structural understanding of prokaryotic gene regulation by redox poise is limited (reviewed in Bauer et al., 1999). One exceptional example is that the significant conformational change triggered by formation of an intramolecular disulfide bond alters DNA recognition by the transcription factor OxyR (Choi et al., 2001; Christman et al., 1989).

To understand the conformational transitions responsible for redox sensing by the Rex family of transcriptional regulators, we have determined the X-ray structure of the Rex homolog from the thermophile *Thermus aquaticus* (T-Rex) bound to NADH at 2.9 Å resolution. The thermostability and minimal size of T-Rex presents an ideal model system for studying the structural mechanism of NADH/NAD^+ sensing by the Rex family of transcriptional repressors. We use electromobility shift (EMSA) and surface plasmon resonance (SPR) assays to show that T-Rex binds DNA in an NADH-responsive manner. NADH but not NAD^+ inhibits DNA binding by T-Rex, indicating that the ability of Rex family members to respond to the redox poise of the NADH/NAD^+ pool is widespread. The X-ray structure reveals a homodimer, with each subunit composed of an NAD(H) binding domain and putative DNA binding domain. Similarities with NAD(H)-dependent dehydrogenases suggest a possible mechanism for allosteric regulation of the Rex/DNA complex formation by NADH.

Results and Discussion

T-Rex DNA Binding Is Inhibited by NADH

Absorbance spectroscopy on purified, recombinant T-Rex indicated that it contained significant amounts of NADH, as judged by an absorbance peak at 340 nm and subsequently by its electron density in the X-ray structure (Figure 2; see below). Since *S. coelicolor* Rex (designated S-Rex hereafter) is unable to bind DNA in the presence of NADH, we attempted to remove NADH from T-Rex by ammonium sulfate precipitation under acidic conditions. The resulting protein had greatly diminished absorbance at 340 nm, indicating that most but not all NADH had been removed (Figure 2A). Since there are currently no known natural targets of T-Rex, the ability to bind to an S-Rex target was tested. As shown in Figure 3A, T-Rex bound to a *S. coelicolor* promoter fragment that contains a ROP site, and the DNA binding activity increased when NADH was depleted. To test if NADH alone inhibited DNA binding, the effect of all four pyridine dinucleotides was investigated (Figure 3B). NADH completely abolished T-Rex/ROP complex formation, whereas NAD^+ and $NADP^+$ had little effect. Surprisingly, although NADPH does not significantly affect the DNA binding activity of S-Rex (Brekasis and Paget, 2003), 1 mM NADPH completely abolished T-Rex/ROP complex formation. At this time, the effect of NADPH on T-Rex is not considered to be physiologically relevant, although further investigation will be required to test this. NADH titration experiments revealed that 100–250 nM NADH caused a 50% loss of the T-Rex/ROP complex (Figure 3C).

SPR experiments were then conducted to determine whether NADH compared with oxidized NAD^+ could actively dissociate the T-Rex/DNA complex (Figure 3D). A biotinylated oligonucleotide containing the ROP site was attached to the streptavidin sensor chip. T-Rex was then bound to the sensor chip in the absence of dinucleotides to give a response unit (RU) shift of ~350 RU. In support of the EMSA data, addition of 1 μM NADH completely dissociated the T-Rex/DNA complex. In contrast, addition of 1 mM NAD^+ had little effect on T-Rex/DNA dissociation but strongly inhibited the ability of NADH to dissociate the T-Rex/DNA complex. Hence, NAD^+ competes with NADH for T-Rex binding, and NAD^+-bound T-Rex retains DNA binding activity, whereas NADH dissociates the T-Rex/DNA complex, as observed for S-Rex (Brekasis and Paget, 2003). The similar sensitivity of T-Rex and S-Rex to NADH/NAD^+ establishes that the mechanism of repressing gene expression in response to the NADH/NAD^+ redox poise is conserved among Rex family members.

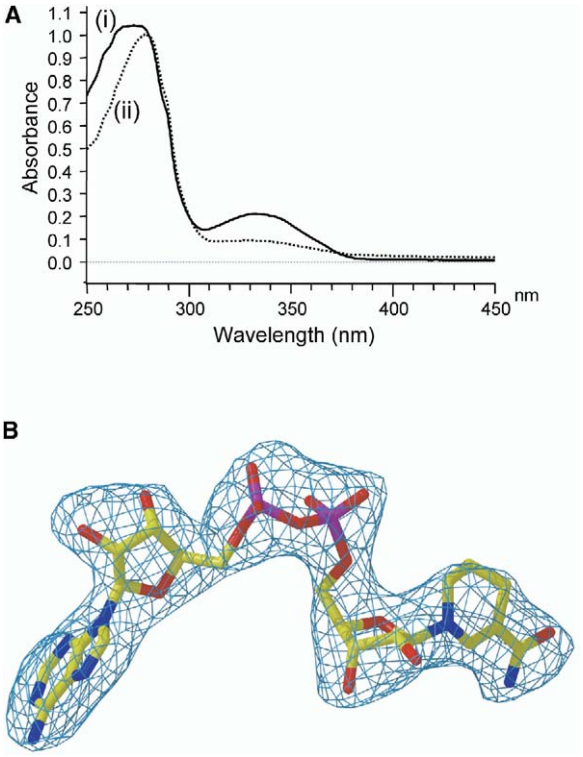

Figure 2. T-Rex Copurified with NADH

(A) Absorption spectrum of purified T-Rex protein before (i) and after (ii) depletion of NADH by acidic ammonium sulfate precipitation. The peak at 340 nm is characteristic of reduced NADH.

(B) Representative omit $|F_{observed}|-|F_{calculated}|$ electron density map for the NADH (contoured at 1.5σ). The NADH molecule, which was omitted from atomic coordinates used for the phase calculation, is represented as a ball-and-stick figure color-coded by atom type (C, yellow; N, blue; O, red; P, purple). Structure representations were prepared by use of BOBSCRIPT (Esnouf, 1997), MOLSCRIPT (Kraulis, 1991), and RASTER3D (Merritt and Bacon, 1997).

Structure Determination

The structure of T-Rex bound to NADH was determined at 2.9 Å resolution using selenomethionine-based multiwavelength anomalous dispersion (MAD) phasing (Hendrickson, 1991) (Table 1). Noncrystallographic symmetry

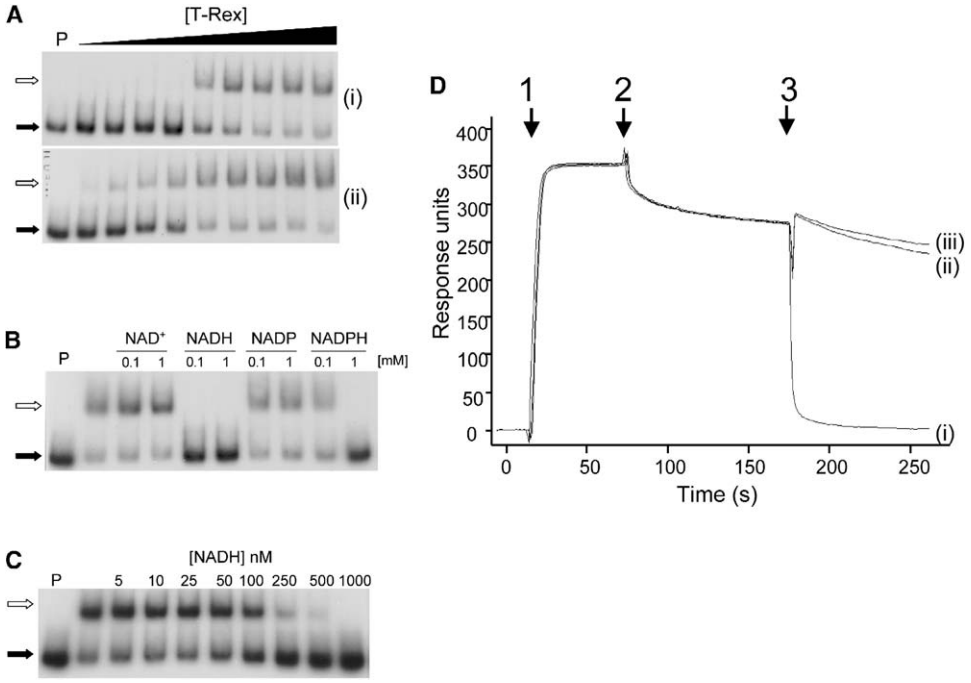

Figure 3. The DNA Binding Activity of T-Rex Is Sensitive to the NADH/NAD+ Redox Poise

(A) Inset: electromobility shift assay (EMSA) using the ROP-containing *rex* promoter fragment (Brekasis and Paget, 2003) as probe and increasing amounts of T-Rex (5 nM, 10 nM, 25 nM, 50 nM, 250 nM, 500 nM, 1 μM, 2.5 μM, and 5μM) prior to (i) or after (ii) depletion of NADH. The closed arrow indicates unbound probe, and the open arrow indicates T-Rex/DNA complex. P, probe alone.

(B) EMSAs were performed as in (A) using 4 μM NADH-depleted T-Rex and 0.1 mM or 1 mM pyridine dinucleotides as indicated.

(C) EMSAs were performed as in (A) using 200 nM NADH-depleted T-Rex and increasing concentrations of NADH.

(D) An SPR sensorgram indicating that NADH but not NAD+ actively dissociates T-Rex from a ROP site. (1) NADH-depleted T-Rex was injected to give a response unit shift of 350 RU, (2) end of T-Rex injection, (3) injection of 1 μM NADH (i), 1 μM NADH + 1mM NAD+ (ii), or 1 mM NAD+ (iii). Sensorgrams were obtained by the subtraction of background values obtained from a DNA-free flow cell from the raw interaction data and then overlayed.

averaging among the seven protein-ligand complexes in the crystallographic asymmetric unit was essential to obtain an interpretable electron density map. The crystallized protein contained bound NADH, based upon the characteristic shape of the electron density and the strong absorbance of the purified protein at 340 nm (Klingenberg, 1963) (Figure 2). Of 211 T-Rex residues, 1–207 were interpretable in some or all of the subunits, whereas residues 4–203 were observed in all copies comprising the asymmetric unit. One subunit appears poorly ordered due to asymmetric interactions at the interface of the dimer found on a crystallographic 2-fold axis and was excluded from detailed structural analyses. A flexible loop region (residues 53–60) was disordered in four of the seven polypeptide chains. Four C-terminal T-Rex residues and three N-terminal residues arising from the protein expression vector were not visible in the experimental electron density map. The final refinement model (crystallographic R factor = 22.8%, free R factor = 27.6%) includes seven 1:1 T-Rex/NADH complexes and five calcium ions located near the NADH phosphates, with excellent stereochemistry (Table 1).

Rex Sequence Comparisons and Homology Models

Previous database searches established that examples of the Rex family are found within the genomes of most gram-positive bacteria (Brekasis and Paget, 2003). Thus, the amino acid sequence of T-Rex is clearly related to homologous proteins encoded by most gram-positive bacteria, including important human pathogens such as *Bacillus anthracis* (34% identity), *Streptococcus pneumoniae* (35% identity), and *Clostridium tetani* (37% identity) (Figure 1A). Homology modeling with MODWEB (Pieper et al., 2004) demonstrates that the T-Rex structure provides relatively accurate homology models (model score ~1.0) for more than 30 Rex family members (>30% identity) and less accurate homology models (model score ≥ 0.7) for 117 more distantly related sequences (≤30% identity). (Models are publicly available from MODBASE [http://alto.compbio.ucsf.edu/modbase] via the advanced search with PDB code 1XCB.) The T-Rex sequence is closely related to the well-characterized *S. coelicolor* S-Rex prototype (Brekasis and Paget, 2003) (45% identity, model score ~1.0). The high level of phylogenetic sequence conservation and excellent model scores indicate that the T-Rex/NADH structure is common to that of S-Rex and other Rex family members.

Structural Overview

The presence of seven T-Rex/NADH complexes in the asymmetric unit of the crystal provides seven indepen-

Table 1. Summary of Data Collection and Refinement Statistics

Crystallographic Data				
Data Set (Wavelength, Å)	Se Inflection (0.9794)	Se Peak[c] (0.9792)	Se Remote (0.9648)	Hg (0.9990)
Diffraction limit (Å)	2.9	2.9	3.0	2.8
Redundancy	3.8	2.6	2.2	2.6
Completeness[a] (%)	99.7 (97.3)	100.0 (100.0)	99.7 (99.8)	97.7 (82.2)
R_{sym}[a,b] (%)	8.7 (32.2)	9.7 (36.4)	10.8 (40.8)	7.8 (32.4)
$< I/\sigma(I) >$[a]	14.9 (4.5)	13.7 (4.0)	9.2 (2.6)	14.4 (4.1)

Refinement Statistics	
No. of atoms	
Protein	11,117
Calcium ions	5
NADH	7 ($C_{21}H_{27}N_7O_{14}P_2$)
R factor[c,d] (%)	
R_{cryst}	22.8
R_{free}	27.6
Rms deviations	
Bond lengths (Å)	0.009
Bond angles (°)	1.5
Overall B factor (Å^2)	33.8

Ramachandran Distributions (%)	
Most favored region	81.6
Additional allowed	17.7
Generously allowed	0.7
Disallowed region	0

[a] Values in parentheses are for the highest-resolution shell, 3.00–2.90 Å for Se peak and inflection data sets, 3.11–3.00 Å for Se remote data, and 2.80–2.90Å for the Hg data.

[b] $R_{sym} = \Sigma_{hkl}\Sigma_i|I_i - <I>|/\Sigma_{hkl}\Sigma_i I_i$, where I_i is an intensity I for the ith measurement of a reflection with indices hkl, and <I> is the weighted mean of all measurements of I.

[c] Data used for refinement.

[d] $R_{cryst} = \Sigma_{hkl}||F_{obs}(hkl)| - k|F_{calc}(hkl)||)/\Sigma_{hkl}|F_{obs}(hkl)|$ for the working set of reflections; R_{free} is R_{cryst} for 7.5% of the reflections excluded from the refinement.

dent views of this redox-sensing transcriptional regulator. The heptameric assembly can be further subdivided into four tight dimers, with one of the dimers straddling a crystallographic 2-fold axis (Supplemental Figure S1). The T-Rex monomer is bilobal, giving rise a butterfly-shaped dimer (Figure 4A) with overall molecular dimensions 60 Å × 50 Å × 30 Å and a central ~12 Å diameter opening. A smaller α/β N-terminal domain (residues 2–76; α1-β1-α2-α3-β2-α4) with similarity to the winged helix (WH) family of transcription factors (reviewed in Gajiwala and Burley, 2000) is connected by a linker region to a larger α/β C-terminal domain (residues 81–187; β3-α5-β4-β5-β6-α6-β7-α7-β8-β9-α8) that has the "Rossmann fold" characteristic of pyridine-nucleotide-dependent dehydrogenases (Rao and Rossmann, 1973). At the C terminus, a "domain-swapped" helix (residues 188–203; α9) inserts into the interdomain cleft of the other subunit, forming the symmetric homodimer. NADH molecules are bound with 1:1 stoichiometry with each C-terminal domain near the dimer interface. The C-terminal NAD(H) binding domains of the subunits are very similar, with pairwise α-carbon root-mean-square differences (rmsd) = 0.4–0.6 Å. The N-terminal WH domains are more variable in structure (pairwise α-carbon rmsds = 0.6–1.3 Å in α-carbon positions) in part due to a flexible glycine-rich loop separating α helix 3 and β strand 2 (residues 53–60) that usually contributes an additional β strand in DNA-bound WH structures. Although the overall topologies of the molecules are similar, the relative orientation of the N- and C-terminal domains varies within the asymmetric unit, as described below (Figure 4B).

The T-Rex Dimer

The T-Rex dimers have an extensive buried surface area (2650 Å^2 per subunit) that is nearly twice that of the largest interdimer interface identified within the crystallographic asymmetric unit (1100 Å^2 per subunit). Accordingly, both T-Rex and S-Rex proteins occur as large dimers (~60 KD), as judged by gel filtration chromatography and dynamic light scattering studies (data not shown). Although the N-terminal WH domains contact one another via their N-terminal α helices, the buried surface area between the WH domains is significantly smaller than expected for established homodimeric structures of comparable size (170 Å^2 versus 500 Å^2, respectively) (Jones and Thornton, 1995). Instead, the C-terminal α helix of each T-Rex monomer contributes the majority of the buried surface area (68%) of the dimer interface by a type of self-association called "three-dimensional domain swapping," in which one polypeptide exchanges a secondary structural element with an identical partner (Bennett et al., 1994) (Figure 5A). The C-terminal α helix is completely buried between the domains of the reciprocal subunit, with one face interacting with side chains displayed on three β strands of the NAD(H) binding domain (β7, β8, β9), whereas the other face packs against the C-terminal tip of the last α helix (α4) in the WH domain and antiparallel to the first α helix (α1). The interdomain linker (residues

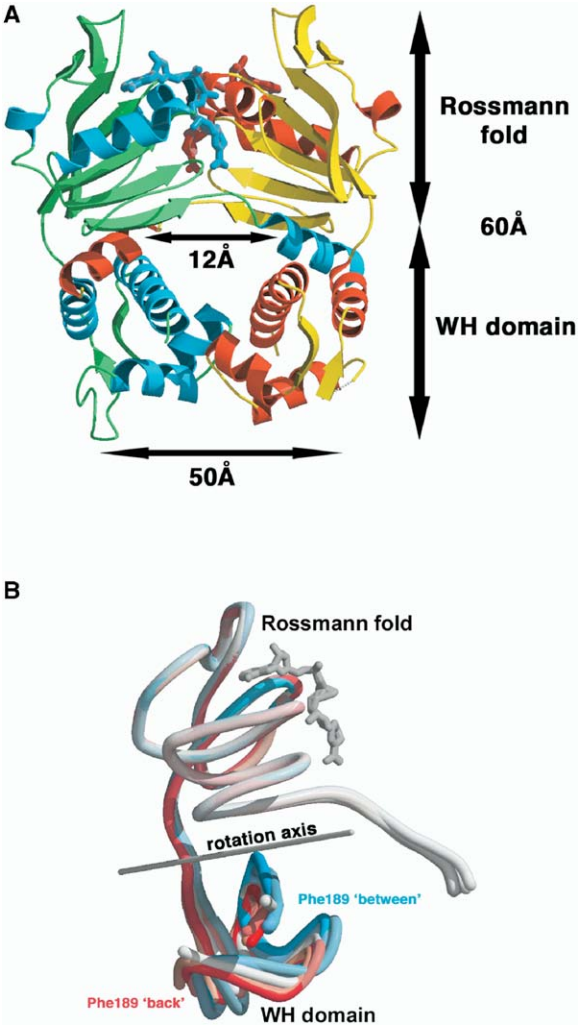

Figure 4. Overall T-Rex Structure and Oligomeric Organization

(A) View of the functional dimer with each subunit colored red/gold or blue/green according to secondary structure (α helices/β sheets). The NAD(H) binding domain (Rossmann fold) and DNA binding (WH) domain are labeled. The A/B dimer is shown in Figures 3–7 and colored identically unless otherwise indicated.

(B) Comparison of the seven independent copies of the T-Rex polypeptide in the asymmetric unit. The subunits were superimposed using the Cα atoms of the C-terminal domain (residues 81–187). The rotation of the N-terminal domain relative to the stationary C-terminal domain is illustrated by a color ramp ranging from blue to white to red. The hinge axis for rotation is indicated with a line. For clarity, a single representative NADH molecule is shown.

77–81) and the loop between α helices α5 and β4 (residues 99–105) encircle the remainder of the C-terminal α helix surface. Conserved features of the C-terminal arm include two leucine residues (Leu193 and Leu196) that interact with hydrophobic residues of the C-terminal NAD(H) binding domain (*Phe105′* and *Ile143′*, respectively; italics indicate residues arising from the other half of the homodimer) and a salt bridge (Asp188-*Arg195′*) formed with the N-terminal WH domain. Additional aromatic residues (Trp205 and Phe198) that appear unique to the T-Rex protein sequence may contribute to thermostability of the *T. aquaticus* dimer.

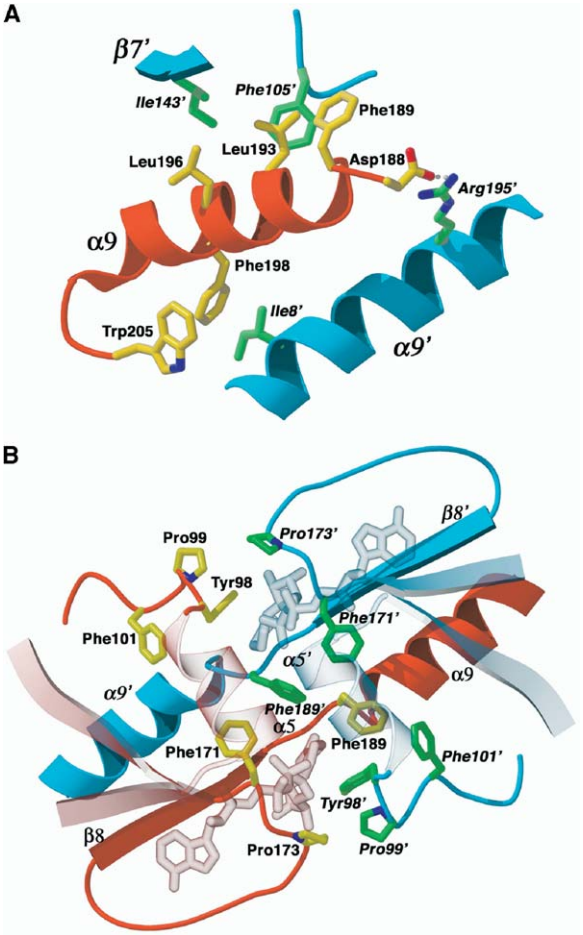

Figure 5. T-Rex Dimer

(A) Interactions mediated by the domain-swapped α helix. Residue labels from the other half of the homodimer are distinguished with primed italics as in the text.

(B) Interactions between the C-terminal domains/NADH molecules of the dimer, viewed down the two-fold axis relating the two NAD(H) binding domains following rotation by 90° about the horizontal axis of Figure 3B.

In addition to the C-terminal α helix, the dimeric conformation is promoted by intersubunit interactions among the first α helix of the Rossmann fold (α5, residues 90–95), a loop segment (residues 96–99), and the two NADH molecules located at the dimer interface (Figure 5B). Both NAD(H) molecules are enclosed by an asymmetric set of aromatic interactions. The parallel planes of the nicotinamide rings at the dimer interface are less than 10 Å apart, permitting intercalation of a single aromatic amino acid side chain. This role is filled by *Phe189′*, which is donated by the linker preceding the C-terminal α helix of one subunit. The *Phe189′* side chain inserts between the NADH molecules, making an edge-to-face interaction with the plane of the nicotinamide ring (70° average interplanar angles). The other faces of the *Phe189′* side chain are packed between the edges of Phe171/*Phe171′* in a "T-shaped" interaction, which is an energetically stabilizing mode of interaction often observed among aromatic side chains

in proteins (Burley and Petsko, 1988). In contrast, Phe189 in the other half of the dimer folds back to pack against *Phe101′* and *Phe171′* in the protein core. The exterior portion of the nicotinamide ring is enclosed by Tyr98, which packs in turn against the preceding Pro99 residue and *Pro173′* of the neighboring molecule. Asymmetric packing interactions among the Phe189 side chains and the nicotinamide rings affects the inclination of the aromatic side chain of *Tyr98′* relative to the major plane of the nicotinamide ring (57° versus 31° average interplanar angle relative to the nicotinamide ring for the intercalated *Phe189′* and back-folded Phe189 conformations, respectively).

The local asymmetry at the NADH binding site propagates into global asymmetry in the relative orientation of the N- and C-terminal domains of the two halves of the homodimer. In subunits with Phe189 inserted between the NAD(H) molecules (designated polypeptide chains A, C, and E; shown in blue in Figure 4B), the N-terminal WH domains are consistently rotated closer to the C-terminal domains than in the subunits with Phe189 folded back into the interior of the protein (designated polypeptide chains B, D, and F; shown in red in Figure 4B). Systematic analyses of interdomain orientations using DynDom (Hayward and Lee, 2002) show that the WH domain is rotated up to 15° relative to the NAD(H) binding domain about an effective hinge axis that occurs between residues 76 and 77 of the linker. The direction of this hinge axis lies approximately parallel to the first α helix of the NAD(H) binding domain (α5 loop, residues 90–99), a region that contributes to the dimer interface and interacts with the nicotinamide ring of the cofactor (Figure 5B). The observation that small differences in the conformation of residues at the NADH binding sites propagates into global rotations of the DNA binding domains provides a mechanism whereby redox sensing alters the DNA binding properties of the homodimer.

The NAD(H) Binding Domain

Despite low pairwise sequence identities between T-Rex and other members of the Rossmann fold family, the core structure and classic dinucleotide interaction motifs are conserved (Lesk, 1995; Rao and Rossmann, 1973). Comparison of the T-Rex C-terminal domain against the Protein Data Bank (www.rcsb.org/pdb) using the DALI server (Holm and Sander, 1993) detected similarity with several NAD(H)-dependent enzymes, including biliverdin reductase (BVR; PDB code 1GCU; Z score, 12.0; rmsd, 3.4 Å; sequence identity, 17% for 120 α-carbon pairs), dihydrodipicolinate reductase (DHPR; PDB code 1DRW; Z score, 10.6; rmsd, 2.8 Å; sequence identity, 13% for 116 α-carbon pairs), and liver alcohol dehydrogenase (LADH; PDB code 2OHX; Z score, 8.5; rmsd, 3.6 Å; sequence identity, 7% for 112 α-carbon pairs). It is remarkable that no similarity with the NAD(H)-responsive CtBP was detected, and structural homology with SIR2 was weak (PDB code 1J8F; Z score, 4.7; rmsd, 3.5 Å; sequence identity, 7% for 94 α-carbon pairs). Conserved T-Rex sequence features that are common to dinucleotide binding proteins include the Gly-X-Gly-X-X-Gly signature sequence of the P loop (T-Rex residues 87–92; Gly-Met-Gly-Arg-Leu-Gly) and a key acidic residue (Asp112) that often discriminates NAD(H) from phosphorylated NADP(H) by interacting with the adenosine 2′ hydroxyl group (Lesk, 1995; Saraste et al., 1990).

Each NADH molecule is bound in an extended conformation similar to that described for other dinucleotide binding domains (Lesk, 1995), with the distinguishing feature that the nicotinamide binding site is located at the T-Rex dimer interface rather than the traditional position between NAD(H) and substrate binding domains of enzyme active sites. The T-Rex NAD(H) dinucleotide binding site can be divided into two distinct sets of interactions (Figures 6A and 6B), one with the adenosine moiety at the loop regions of the C-terminal domain, and the other with the nicotinamide portion of the effector molecule bound to the opposing subunit. The adenine base of the dinucleotide is sandwiched between the hydrophobic side chains of two loop residues (Val113 and Val148), with the amines at the base edge in a relatively solvent-exposed position. The α-carbon of the first glycine (Gly87) in the P loop makes van der Waals contact with the opposite edge of the adenine base (average Cα-N3 distance is 3.7 Å). The NADH pyrophosphate moiety interacts with the P loop Gly89, Arg90, and N terminus of α helix 5. Mutation of the corresponding S-Rex glycine residue (S-Rex-Gly102, T-Rex Gly89) to Ala eliminated NADH-dependent modulation of DNA binding (Brekasis and Paget, 2003). The final glycine of the P loop (Gly92) forms a sharp turn that initiates α helix 5. *Tyr98′* from the other half of the homodimer faces the nicotinamide *pro-R* hydrogen and completely masks the nicotinamide from solvent. As described above, an asymmetric array of hydrophobic residues fill the region between the nicotinamide rings at the dimer interface. Although most of the NADH contacts are similar within distinct subunits, a preferential hydrogen bond is formed between the carboxamide oxygen and the backbone of the *Phe189′* side chain (Figure 6A).

When the structure of T-Rex is compared with NAD(H)-dependent enzymes such as LADH (Eklund et al., 1981) bound to inhibitors, the *Tyr98′* side chain occupies the location of bound substrates (Figure 6C). Although the *Tyr98′* directly interacts with the reduced carbon of the nicotinamide ring (average NC4-Cδ1 distance is 3.8 Å), it appears highly unlikely that the aromatic side chain could serve as a substrate for the bound NADH, given the mechanistic and energetic difficulty of reducing the phenol-like ring (Boll et al., 2002) and the reduced spectral characteristics of the bound NADH (Klingenberg, 1963). No cavities for entry of other substrates are observed in the vicinity of the NAD(H) binding site (using the program Voidoo [Kleywegt and Jones, 1994] with 1.4 Å water molecule probe radius). During substrate reduction by LADH, kinetic and structural analyses indicate that a bound Zn^{+2} ion plus histidine and serine side chains stabilize and facilitate protonation of an anionic intermediate (Eklund et al., 1982; LeBrun et al., 2004; Leskovac et al., 1999). In contrast, polar functional groups are conspicuously absent in the tight hydrophobic pocket that encloses the nicotinamide ring in T-Rex. These results indicate that T-Rex is unlikely to have enzymatic activity.

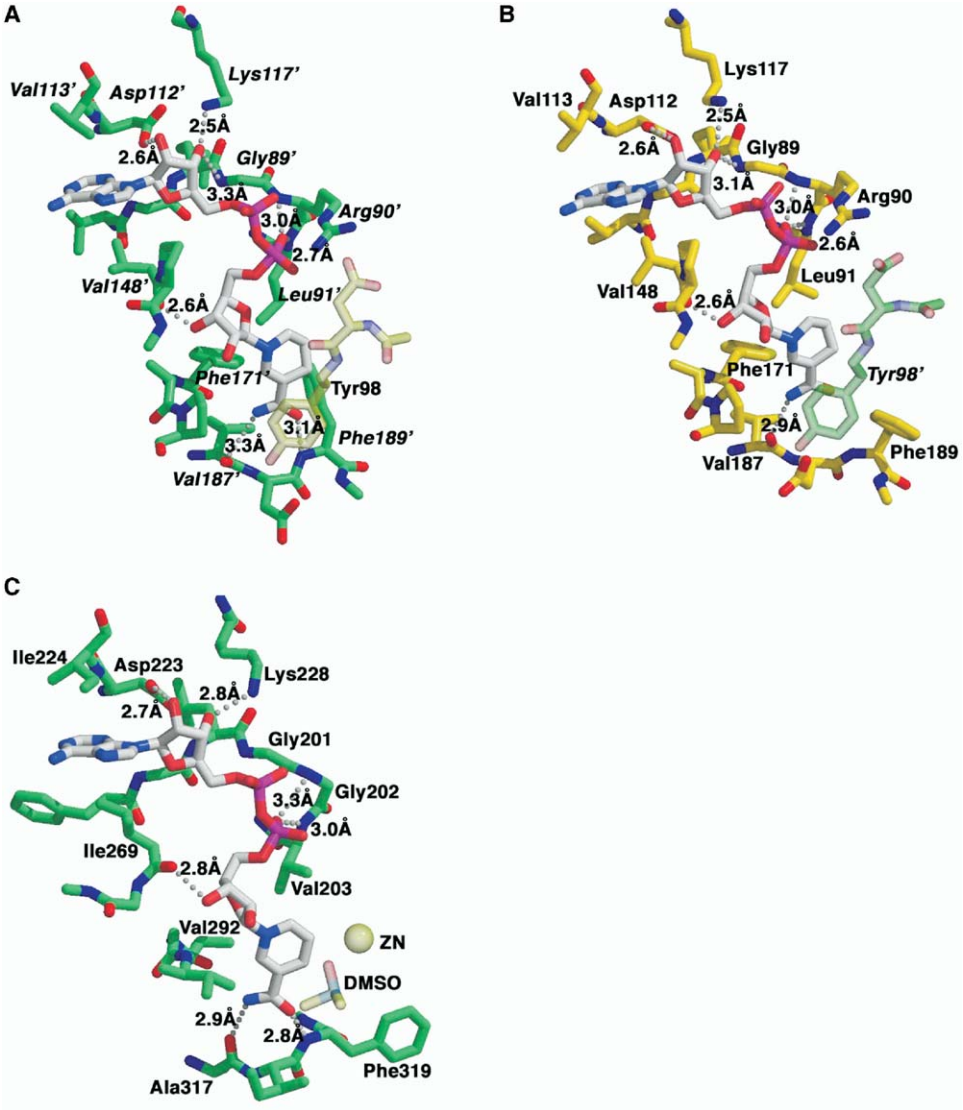

Figure 6. The T-Rex NAD(H) Binding Sites and Comparison with NAD(H)-Dependent Dehydrogenase

(A) T-Rex interactions with the NADH effector molecule, in the conformation with Phe189 inserted between the nicotinamide rings. Average distances between interacting atoms of the three subunits exhibiting this conformation are indicated.

(B) T-Rex interactions with the *NADH′* molecule bound to the opposite subunit, in the conformation with Phe189 folded back and buried within the hydrophobic core.

(C) LADH interactions with bound NADH, zinc ion (ZN), and DMSO substrate.

The Winged Helix Domain

The DNA binding properties of T-Rex almost certainly stem from the presence of the N-terminal domain, because fusion with an N-terminal peptide inhibits DNA binding (Du and Pene, 1999). Accordingly, the N-terminal domain of T-Rex (residues 2–76) displays structural similarity with several DNA binding proteins that contain HTH motifs or are members of the WH subfamily, although the relationships are less striking than the clear Rossmann fold of the T-Rex C-terminal domain. The most similar structures detected using the DALI server (Holm and Sander, 1993) include double-stranded RNA-specific adenosine deaminase (ADAR1; PDB code 1QBJ; Z score, 5.8; rmsd, 2.6 Å; sequence identity, 14% for 59 α-carbon pairs), LexA repressor (LexA; PDB code 1LEA; Z score, 4.4; rmsd, 2.5 Å; sequence identity, 5% for 59 α-carbon pairs), tetracycline repressor (TetR; PDB code 2TCT; Z score, 3.8; rmsd, 2.9 Å; sequence identity, 13% for 54 α-carbon pairs), and the fatty acid metabolism regulator (FadR; PDB code 1E2X; Z score, 3.7; rmsd, 3.1 Å; sequence identity, 17% for 63 α-carbon pairs). The (α1-β1-α2-α3-β2) T-Rex subdomain displays reasonable similarity with a WH motif (topology α1-β1-α2-α3-β2-W-β3, where W separates the β strands of the "wing"). The T-Rex HTH submotif (α2-α3) displays a packing angle (102°) that is characteristic of the WH subfamily, rather than the 120° value typically observed for HTH proteins (Gajiwala and Burley, 2000). However, the normal wing β strand pattern of hydrogen bonds is distorted among three of the seven copies of T-Rex found in the asymmetric unit and completely disordered among the remaining four copies. These devia-

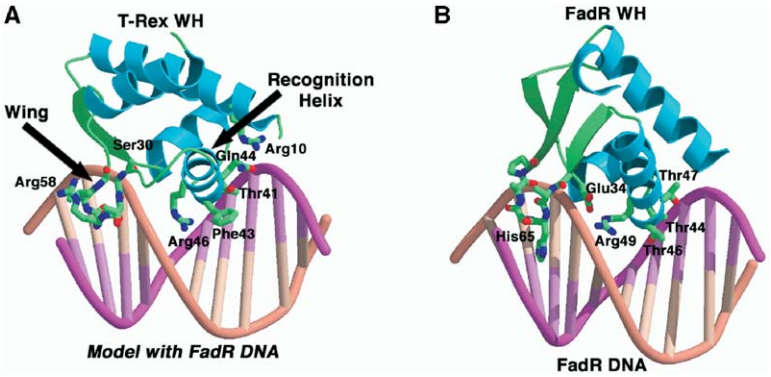

Figure 7. Model for T-Rex/DNA Recognition

(A) T-Rex WH domain docked with DNA operator from FadR/DNA (PDB code 1HW2) based upon superposition of matching Cα positions. Putative interacting residues are shown with ball-and-stick representations. The DNA strands and base pairs are shown as a coil.

(B) View of FadR/DNA complex for comparison.

tions from the structure of a canonical WH motif appear to result from the inherent flexibility of a Gly-rich region within the T-Rex wing (residues 54–57). It is remarkable that the conformation of the Gly-rich wing is correlated with the asymmetry of the NAD(H) binding sites. The wing appears disordered in the three subunits in which Phe189 is folded back into the protein interior, but is readily visible in the three subunits in which *Phe189′* is inserted between the NADH molecules at the dimer interface.

Insights into the possible mode of T-Rex/DNA recognition are available from comparison of T-Rex with similar structures of WH or HTH/DNA complexes. For most WH or HTH motifs, sequence-specific DNA contacts are formed by a so-called "recognition helix" positioned within the DNA major groove (Gajiwala and Burley, 2000; Huffman and Brennan, 2002). When the T-Rex WH domain is docked into a protein-DNA complex using previously experimental structures of the WH-containing protein FadR bound to DNA (van Aalten et al., 2001; Xu et al., 2001), the recognition helix (α3) fits in the major groove, with the side chains of T-rex residues Thr41, Phe43, and Gln44 (corresponding to S-Rex Asn54, Ala56, and Lys57) positioned on one face of the α helix near the edges of the base pairs (Figure 7). Adjacent to the recognition helix, a Gly-rich T-Rex region corresponding to the FadR wing turns over the sugar-phosphate backbone and intrudes into the DNA minor groove. The wing of most WH-containing proteins increases DNA binding affinity without necessarily affecting specificity (Gajiwala and Burley, 2000). Accordingly, the Gly-rich T-Rex sequence (residues 53–62) is highly conserved among Rex homologs (consensus [Gly-X-X-Gly-X-(Arg/Lys)-Gly-X-Gly-Tyr]), in contrast with the relatively divergent residues of the recognition helix that could discriminate different operator sequences. In addition, a few conserved Rex residues, including Arg46, Ser30, and Arg10, appear capable of making nonspecific contacts with the phosphate backbone in an analogous manner to the corresponding residues found in FadR and TetR.

Model for Redox Sensing

S-Rex regulates transcription of several respiratory genes by responding to changes in the NADH/NAD^+ ratio, since NADH but not NAD^+ inhibits S-Rex operator DNA binding (Brekasis and Paget, 2003). Given high sequence identity with S-Rex (45% identity), our T-Rex/NADH costructure almost certainly represents the conformation of the protein with low affinity for DNA. The recognition helices of the four independent T-Rex dimers observed in our crystals are related by a 154–161° relative rotation and 13–17 Å relative translation, which is incompatible with the requirement for a 180° relative rotation and 27 Å relative translation between separate palindromic octameric half-sites of the Rex operator (assuming canonical B-form DNA). This geometric incompatibility is visible from the results of our docking study, which demonstrates that one of the T-Rex WH motifs in the NADH-bound conformation would be predicted to make a steric clash with the DNA backbone using either the FadR (van Aalten et al., 2001; Xu et al., 2001) or the TetR operators (Orth et al., 2000). By analogy with other transcriptional regulatory systems (Huffman and Brennan, 2002), it is likely that replacing the effector NADH with NAD^+ would induce significant conformational changes in the T-Rex dimer that would enable DNA recognition.

Although conformational changes are difficult to predict, comparison of the T-Rex structure with the classic substrate-induced domain closure of liver alcohol dehydrogenase (LADH) may indicate which residues play critical roles in NAD(H)-regulated DNA binding. In LADH, the NAD(H) cofactor and the alcohol/aldehyde substrates bind the C-terminal and N-terminal domains, respectively, giving rise to local conformational changes that close the active site by propagating a relative 10° rigid-body rotation of the domains (Colonna-Cesari et al., 1986; Hayward, 2004). When the NAD(H) binding domains of T-Rex and LADH are superimposed (1.9 Å rmsd for 63 equivalent α-carbon atoms), the LADH active site is located at the T-Rex dimerization interface, where the LADH substrate binding domain overlaps one of the T-Rex subunits (Figure 6C). Since the LADH active site opens in the absence of NAD(H), this observation suggests that the T-Rex subunits may shift apart when NADH is removed.

LADH-Val294 undergoes one of the largest movements among the active site residues of the LADH apoenzyme versus substrate/NADH-bound forms (Eklund et al., 1981), swinging 6 Å (Cγ-holo-Cγ-apo) to interact with substrate bound to the active site. In our T-Rex structure, a highly conserved proline (*Pro173′*) corresponds to LADH-Val294. This T-Rex *Pro173′* packs

against the Tyr98 side chain, which in turn occupies the position of LADH substrate. As described above, the packing angle between the side chain of Tyr98 and the nicotinamide ring varies according to the asymmetric conformations of Phe189/*Phe189′* in the two halves of the homodimer. More dramatic changes can be envisioned upon side chain π-stacking with a planar, charged NAD^+ versus a puckered NADH ring. Alternatively, the charge or pucker of the nicotinamide ring may alter the direction of the domain-swapped α helix, for example by electrostatic repulsion of the N terminus of the α helix (Hol, 1985). Since this domain-swapped α helix forms the major interface between the effector binding and DNA binding domains, reorientation could alter the position of the DNA binding domain of the other dimer subunit and thereby modulate its nucleic acid binding properties.

Universal themes and intriguing differences are observed among structures of transcription factors bound to their small molecule effectors or DNA operators (Huffman and Brennan, 2002; Orth et al., 2000; Saenger et al., 2000; van Aalten et al., 2001, 2000; Xu et al., 2001). Although the details of the allosteric transitions vary considerably, it is clear that small local conformational changes within an effector binding domain can be amplified throughout the tertiary structure of the transcription factor to alter the relative disposition of the DNA binding domains. In such cases, the effector often inhibits DNA binding of a dimeric transcription factor by increasing the distance separating the DNA binding domains, resulting in a clash with the DNA double helix. The structure of the T-Rex/NADH complex suggests that Rex family members may employ a novel variation on this theme, in which bound NADH dissociates Rex from the target operator site by reducing the intradimer distance between the WH motifs in a manner analogous with enzymatic domain closure. Full evaluation of this model for redox sensing by Rex family members must await further mutagenesis and structures of Rex in the NAD^+- and DNA-bound states.

Experimental Procedures

EMSA and SPR Experiments

The T-Rex protein was expressed as described in the *E. coli* strain BL21 (Du and Pene, 1999) and purified by anion-exchange, cation-exchange, and heparin-affinity chromatography. For DNA binding studies, NADH was depleted from T-Rex preparations by precipitation using an acidified (pH 3.0) saturated ammonium sulfate solution followed by extensive dialysis, as described (Gomi et al., 1990). For EMSAs, the *rex* promoter probe was generated by PCR, 5′ end labeled using [γ-^{32}P]ATP, and reactions were performed as described (Brekasis and Paget, 2003). SPR experiments were conducted in HBS-T buffer (10 mM HEPES [pH 7.4], 150 mM NaCl, 3.4 mM EDTA, 0.005% Tween-20) using a BIAcore 2000 instrument (BIAcore AB, Uppsala, Sweden) at a flow rate of 20 μl/minute. The target was a biotinylated 37 bp double-stranded oligonucleotide containing the ROP site that lies upstream of the *S. coelicolor nuoA* gene (Brekasis and Paget, 2003). NADH-depleted T-Rex was prebound to the DNA by injecting 6 μM aliquots to give a final increase of ~350 RU. NADH and/or NAD^+ made up in HBS-T were then injected, and the change in RU was monitored over time.

Crystallization and Structure Determination

A solution of protein (1 μl of 25 mg/ml) containing 100 mM NaCl and 15 mM N-2-hydroxyethylpiperazine-N′-2-ethanesulfonic acid (HEPES) was mixed with 1 μl of reservoir solution containing 30%(v/v) PEG400, 200 mM $CaCl_2$, 100 mM HEPES (pH 7.5) and equilibrated by the hanging drop vapor diffusion method against 0.6 ml of the same reservoir solution at 4°C. Crystals appeared after 2 weeks. Se-Met-labeled protein was expressed and crystallized in a similar manner. Crystals belong to monoclinic space group C2 (unit cell dimensions a = 189 Å, b = 89 Å, c = 113 Å, β = 106°) with seven polypeptide chains per asymmetric unit. Three multiwavelength anomalous dispersion (MAD) data sets were collected from cryogenically cooled crystals in the vicinity of the Se K-absorption edge (Hendrickson, 1991) at Beamline X9A (National Synchrotron Light Source, Brookhaven National Laboratory). A fourth data set was obtained near the Hg L(III)-absorption edge from an S-Met crystal soaked in 0.5 mM ethyl-mercuric phosphate for 4 hr. Data were processed using Denzo/Scalepack (Otwinowski and Minor, 1997), and initial heavy atom sites were located using SnB (Weeks and Miller, 1999). Unless otherwise indicated, crystallographic manipulations were carried out using CCP4 (1994). The initial overall figure of merit (FoM) of 0.30 at 2.9 Å resolution was improved by iterative density modification and noncrystallographic symmetry averaging among the C- or N-terminal domains of three dimers to provide an interpretable electron density map (FoM = 0.82). The seventh molecule lies on a crystallographic two-fold, and asymmetric residues at the NAD(H) binding site are poorly ordered. The polypeptide chain structure was built manually using the program O (Jones et al., 1991) and refined using CNS (Brunger et al., 1998). The NADH dinucleotide bound to each monomer was readily identified from difference electron density maps and interpreted as the reduced form based upon distinctive absorbance of purified T-Rex protein at 340 nM (Klingenberg, 1963). Structure determination and final refinement statistics are given in Table 1.

Supplemental Data

Supplemental Data are available at http://www.structure.org/cgi/content/full/13/1/43/DC1/.

Acknowledgments

At the NSLS, we thank Dr. K.R. Rajashankar for assistance using Beamline X9A. We are grateful to Dr. X. Du for providing the pTP253 expression plasmid. We thank Dr. R.L. McMacken, L. Mull, and Dr. J.E. Wedekind for insightful discussions. This structure was determined and initially refined as target T744 in the Burley Laboratory at The Rockefeller University under the auspices of the NIGMS funded Protein Structure Initiative by the New York Structural Genomics Research Consortium supported by an NIH Center Grant P50 GM-62529 (S.K.B.). Details of the refinement and subsequent functional analysis were completed collaboratively between the Kielkopf Laboratory at Johns Hopkins University and the Paget Laboratory at University of Sussex. E.A.S. is a Calvin A. Lang Fellow. S.K.B. was also a member of the Howard Hughes Medical Institute. Work in the Paget Laboratory was supported by BBSRC grant P19928.

Received: September 10, 2004
Revised: October 17, 2004
Accepted: October 28, 2004
Published: January 11, 2005

References

Avalos, J.L., Celic, I., Muhammad, S., Cosgrove, M.S., Boeke, J.D., and Wolberger, C. (2002). Structure of a SIR2 enzyme bound to an acetylated p53 peptide. Mol. Cell *10*, 523–535.

Avalos, J.L., Boeke, J.D., and Wolberger, C. (2004). Structural basis for the mechanism and regulation of SIR2 enzymes. Mol. Cell *13*, 639–648.

Bauer, C.E., Elsen, S., and Bird, T.H. (1999). Mechanisms for redox control of gene expression. Annu. Rev. Microbiol. *53*, 495–523.

Bennett, M.J., Choe, S., and Eisenberg, D. (1994). Domain swap-

ping: entangling alliances between proteins. Proc. Natl. Acad. Sci. USA *91*, 3127–3131.

Blander, G., and Guarente, L. (2004). The SIR2 family of protein deacetylases. Annu. Rev. Biochem. *73*, 417–435.

Boll, M., Fuchs, G., and Heider, J. (2002). Anaerobic oxidation of aromatic compounds and hydrocarbons. Curr. Opin. Chem. Biol. *6*, 604–611.

Brekasis, D., and Paget, M.S.B. (2003). A novel sensor of NADH/NAD+ redox poise in *Streptomyces coelicolor* A3(2). EMBO J. *22*, 4856–4865.

Brook, I. (2002). Anaerobic infections in children. Microbes Infect. *4*, 1271–1280.

Brunger, A.T., Adams, P.D., Clore, G.M., DeLano, W.L., Gros, P., Grosse-Kunstleve, R.W., Jiang, J.S., Kuszewski, J., Nilges, M., Pannu, N.S., et al. (1998). Crystallography & NMR system: A new software suite for macromolecular structure determination. Acta Crystallogr. D Biol. Crystallogr. *54*, 905–921.

Burley, S.K., and Petsko, G.A. (1988). Weakly polar interactions in proteins. Adv. Protein Chem. *39*, 125–189.

CCP4 (Collaborative Computational Project, Number 4) (1994). The CCP4 suite: programs for protein crystallography. Acta Crystallogr D Biol. Crystallogr. *50*, 760–763.

Chang, J.H., Kim, H.C., Hwang, K.Y., Lee, J.W., Jackson, S.P., Bell, S.D., and Cho, Y. (2002). Structural basis for the NAD-dependent deacetylase mechanism of SIR2. J. Biol. Chem. *277*, 34489–34498.

Choi, H., Kim, S., Mukhopadhyay, P., Cho, S., Woo, J., Storz, G., and Ryu, S. (2001). Structural basis of the redox switch in the OxyR transcription factor. Cell *105*, 103–113.

Christman, M.F., Storz, G., and Ames, B.N. (1989). OxyR, a positive regulator of hydrogen peroxide-inducible genes in Escherichia coli and Salmonella typhimurium, is homologous to a family of bacterial regulatory proteins. Proc. Natl. Acad. Sci. USA *86*, 3484–3488.

Colonna-Cesari, F., Perahia, D., Karplus, M., Eklund, H., Braden, C.I., and Tapia, O. (1986). Interdomain motion in liver alcohol dehydrogenase. Structural and energetic analysis of the hinge bending mode. J. Biol. Chem. *261*, 15273–15280.

Dixon, R., and Kahn, D. (2004). Genetic regulation of biological nitrogen fixation. Nat. Rev. Microbiol. *2*, 621–631.

Du, X., and Pene, J. (1999). Identification, cloning and expression of p25, an AT-rich DNA-binding protein from the extreme thermophile, *Thermus aquaticus* YT-1. Nucleic Acids Res. *27*, 1690–1697.

Eklund, H., Samma, J.P., Wallen, L., Branden, C.I., Akeson, A., and Jones, T.A. (1981). Structure of a triclinic ternary complex of horse liver alcohol dehydrogenase at 2.9 A resolution. J. Mol. Biol. *146*, 561–587.

Eklund, H., Plapp, B.V., Samama, J.P., and Branden, C.I. (1982). Binding of substrate in a ternary complex of horse liver alcohol dehydrogenase. J. Biol. Chem. *257*, 14349–14358.

Esnouf, R.M. (1997). An extensively modified version of MolScript that includes greatly enhanced coloring capabilities. J. Mol. Graph. Model. *15*, 132–134.

Finnin, M.S., Donigian, J.R., and Pavletich, N.P. (2001). Structure of the histone deacetylase SIR2. Nat. Struct. Biol. *8*, 621–625.

Flores, E.R., Perez, F., and de la Torre, M. (1997). Scale-up of *Bacillus thuringiensis* fermentation based on oxygen transfer. J. Ferment. Bioeng. *83*, 561–564.

Gajiwala, K.S., and Burley, S.K. (2000). Winged helix proteins. Curr. Opin. Struct. Biol. *10*, 110–116.

Georgellis, D., Kwon, O., and Lin, E.C. (2001). Quinones as the redox signal for the arc two-component system of bacteria. Science *292*, 2314–2316.

Gomi, T., Takata, Y., Date, T., Fujioka, M., Aksamit, R.R., Backlund, P.S., Jr., and Cantoni, G.L. (1990). Site-directed mutagenesis of rat liver S-adenosylhomocysteinase. Effect of conversion of aspartic acid 244 to glutamic acid on coenzyme binding. J. Biol. Chem. *265*, 16102–16107.

Hayward, S. (2004). Identification of specific interactions that drive ligand-induced closure in five enzymes with classic domain movements. J. Mol. Biol. *339*, 1001–1021.

Hayward, S., and Lee, R.A. (2002). Improvements in the analysis of domain motions in proteins from conformational change: DynDom version 1.50. J. Mol. Graph. Model. *21*, 181–183.

Hendrickson, W.A. (1991). Determination of macromolecular structures from anomalous diffraction of synchrotron radiation. Science *254*, 51–58.

Hol, W.G. (1985). Effects of the α-helix dipole upon the functioning and structure of proteins and peptides. Adv. Biophys. *19*, 133–165.

Holm, L., and Sander, C. (1993). Protein structure comparison by alignment of distance matrices. J. Mol. Biol. *233*, 123–138.

Huffman, J.L., and Brennan, R.G. (2002). Prokaryotic transcription regulators: more than just the helix-turn-helix motif. Curr. Opin. Struct. Biol. *12*, 98–106.

Jones, S., and Thornton, J.M. (1995). Protein-protein interactions: a review of protein dimer structures. Prog. Biophys. Mol. Biol. *63*, 31–65.

Jones, T.A., Zou, J.Y., Cowan, S.W., and Kjeldgaard, G. (1991). Improved methods for building protein models in electron density maps and the location of errors in these models. Acta Crystallogr. A *47*, 110–119.

Jordan, P.A., Thomson, A.J., Ralph, E.T., Guest, J.R., and Green, J. (1997). FNR is a direct oxygen sensor having a biphasic response curve. FEBS Lett. *416*, 349–352.

Khoroshilova, N., Popescu, C., Munck, E., Beinert, H., and Kiley, P.J. (1997). Iron-sulfur cluster disassembly in the FNR protein of *Escherichia coli* by O_2: [4Fe-4S] to [2Fe-2S] conversion with loss of biological activity. Proc. Natl. Acad. Sci. USA *94*, 6087–6092.

Kleywegt, G.J., and Jones, T.A. (1994). Detection, delineation, measurement and display of cavities in macromolecular structures. Acta Crystallogr. *D50*, 178–185.

Klingenberg, M. (1963). Detection, delineation, measurement and display of cavities in macromolecular structures. In Methods of Enzymatic Analysis, H.U. Bergmeyer, ed. (New York: Academic Press), pp. 531–537.

Kraulis, P.J. (1991). MOLSCRIPT: A program to produce both detailed and schematic plots of protein structures. J. Appl. Crystallogr. *24*, 946–950.

Kumar, V., Carlson, J.E., Ohgi, K.A., Edwards, T.A., Rose, D.W., Escalante, C.R., Rosenfeld, M.G., and Aggarwal, A.K. (2002). Transcription corepressor CtBP is an NAD(+)-regulated dehydrogenase. Mol. Cell *10*, 857–869.

LeBrun, L.A., Park, D.H., Ramaswamy, S., and Plapp, B.V. (2004). Participation of histidine-51 in catalysis by horse liver alcohol dehydrogenase. Biochemistry *43*, 3014–3026.

Lesk, A.M. (1995). NAD-binding domains of dehydrogenases. Curr. Opin. Struct. Biol. *5*, 775–783.

Leskovac, V., Trivic, S., Anderson, B.M., Urbauer, J.L., Bradshaw, D.E., and Cleland, W.W. (1999). Comparison of the chemical mechanisms of action of yeast and equine liver alcohol dehydrogenase. Eur. J. Biochem. *264*, 840–847.

Merritt, E.A., and Bacon, D.J. (1997). Raster3D: photorealistic molecular graphics. Methods Enzymol. *277*, 505–524.

Min, J., Landry, J., Sternglanz, R., and Xu, R.M. (2001). Crystal structure of a SIR2 homolog-NAD complex. Cell *105*, 269–279.

Murdoch, D.A. (1998). Gram-positive anaerobic cocci. Clin. Microbiol. Rev. *11*, 81–120.

Nardini, M., Spano, S., Cericola, C., Pesce, A., Massaro, A., Millo, E., Luini, A., Corda, D., and Bolognesi, M. (2003). CtBP/BARS: a dual-function protein involved in transcription co-repression and Golgi membrane fission. EMBO J. *22*, 3122–3130.

Orth, P., Schnappinger, D., Hillen, W., Saenger, W., and Hinrichs, W. (2000). Structural basis of gene regulation by the tetracycline inducible Tet repressor-operator system. Nat. Struct. Biol. *7*, 215–219.

Otwinowski, Z., and Minor, W. (1997). Processing of X-ray diffraction data in oscillation mode. Methods Enzymol. *276*, 307–326.

Park, H.D., Guinn, K.M., Harrell, M.I., Liao, R., Voskuil, M.I., Tompa, M., Schoolnik, G.K., and Sherman, D.R. (2003). Rv3133c/dosR is a transcription factor that mediates the hypoxic response of Mycobacterium tuberculosis. Mol. Microbiol. *48*, 833–843.

Patschkowski, T., Bates, D.M., and Kiley, P.J. (2000). Mechanisms for sensing and responding to oxygen deprivation. In Bacterial Stress Responses, G. Storz and R. Hengge-Aronis, eds. (Washington, DC: ASM Press), pp. 61–78.

Pieper, U., Eswar, N., Braberg, H., Madhusudhan, M.S., Davis, F.P., Stuart, A.C., Mirkovic, N., Rossi, A., Marti-Renom, M.A., Fiser, A., et al. (2004). MODBASE, a database of annotated comparative protein structure models, and associated resources. Nucleic Acids Res. *32*, D217–D222.

Rao, S.T., and Rossmann, M.G. (1973). Comparison of super-secondary structures in proteins. J. Mol. Biol. *76*, 241–256.

Saenger, W., Orth, P., Kisker, C., Hillen, W., and Hinrichs, W. (2000). The tetracycline repressor: a paradigm for a biological switch. Angew. Chem. Int. Ed. Engl. *39*, 2042–2052.

Saraste, M., Sibbald, P.R., and Wittinghofer, A. (1990). The P-loop: a common motif in ATP- and GTP-binding proteins. Trends Biochem. Sci. *15*, 430–434.

Sassi, H., Deschamps, A.M., and Lebeault, J.M. (1996). Process analysis of L-lysine fermentation with *Corynebacterium glutamicum* under different oxygen and carbon dioxide supplies and redox potentials. Process Biochem. *31*, 493–497.

Taylor, B.L., Zhulin, I.B., and Johnson, M.S. (1999). Aerotaxis and other energy-sensing behavior in bacteria. Annu. Rev. Microbiol. *53*, 103–128.

van Aalten, D.M., DiRusso, C.C., Knudsen, J., and Wierenga, R.K. (2000). Crystal structure of FadR, a fatty acid-responsive transcription factor with a novel acyl coenzyme A-binding fold. EMBO J. *19*, 5167–5177.

van Aalten, D.M., DiRusso, C.C., and Knudsen, J. (2001). The structural basis of acyl coenzyme A-dependent regulation of the transcription factor FadR. EMBO J. *20*, 2041–2050.

Van Hamme, J.D., Singh, A., and Ward, O.P. (2003). Recent advances in petroleum microbiology. Microbiol. Mol. Biol. Rev. *67*, 503–549.

Weeks, C.M., and Miller, R. (1999). Optimizing Shake-and-Bake for proteins. Acta Crystallogr. D Biol. Crystallogr. *55*, 492–500.

Williamson, D.H., Lund, P., and Krebs, H.A. (1967). The redox state of free nicotinamide-adenine dinucleotide in the cytoplasm and mitochondria of rat liver. Biochem. J. *103*, 514–527.

Xu, Y., Heath, R.J., Li, Z., Rock, C.O., and White, S.W. (2001). The FadR.DNA complex. Transcriptional control of fatty acid metabolism in *Escherichia coli*. J. Biol. Chem. *276*, 17373–17379.

Zhang, W., and Phillips, G.N., Jr. (2003). Structure of the oxygen sensor in *Bacillus subtilis*: signal transduction of chemotaxis by control of symmetry. Structure *11*, 1097–1110.

Zhao, K., Chai, X., Clements, A., and Marmorstein, R. (2003a). Structure and autoregulation of the yeast Hst2 homolog of SIR2. Nat. Struct. Biol. *10*, 864–871.

Zhao, K., Chai, X., and Marmorstein, R. (2003b). Structure of the yeast Hst2 protein deacetylase in ternary complex with 2′-O-acetyl ADP ribose and histone peptide. Structure *11*, 1403–1411.

Accession Numbers

Atomic coordinates and experimental structure factors have been deposited in the Protein Data Bank under ID code 1XCB.